Coupling of Lateral Electric Field and Transversal Faradaic Processes at the Conductor/Electrolyte Solution Interface

J. F. L. Duval,*,† M. Minor,‡ J. Cecilia,§ and H. P. van Leeuwen†

Department of Physical Chemistry and Colloid Science, Wageningen University, Dreijenplein 6, 6703 HB Wageningen, The Netherlands, NIZO Research Institute, Kernhemseweg 2, 6718 ZB Ede, The Netherlands, and Departament de Matematica, Universitat de Lleida, Rovira Roure 177, 25198 Lleida, Spain

Received: November 20, 2002; In Final Form: February 5, 2003

A quantitative theory is presented for the bipolar behavior of conducting planar surfaces in a thin-layer cell of a type commonly used in electrokinetic studies. The lateral current density distribution in the cell, as dictated by the externally applied field in the solution, is formulated for the situation in which depolarization of the interface arises from transversal electron-transfer processes that occur at the two sides of the conducting surface. The treatment explicitly analyses the two limiting cases of bipolar electrodic behavior, i.e., totally irreversible electron transfer and Nernstian (mass-transfer-limited) electrodics. The spatial distribution of the electric field is calculated by means of Poisson's equation under conditions of a finite current. The results allow for a rigorous estimation of the overall bipolar faradaic current. Analytical expressions are given for the electric parameters (potential, field, local current, and bipolar faradaic current) in the case of irreversible electron transfer, and numerical analysis is performed for the reversible, Nernstian case. Deviations of the conductivity curves from the trend expected on the basis of a linear potential profile are discussed in terms of the local ohmic and faradaic contributions to the total current. The theory is supported and illustrated by experimental data for gold and aluminum surfaces in KNO_3 solution, in the absence and presence of the electroactive species $Fe(CN)_6^{3-}/Fe(CN)_6^{4-}$.

1. Introduction

The bipolar behavior of electroconductive objects isolated between two current feeders and subjected to an external electric field has been discussed extensively in many areas, including the dissolution of nuclear fuel,[1] control of oxide film thickness,[2] organic synthesis,[3−6] corrosion, etc. The bipolar behavior has also been investigated in the specific context of electrochemistry at dispersed microelectrodes.[6,7] The geometry of microsphere electrodes, which allows for the development of spherical diffusion fields in the bulk of the surrounding solution, presents multiple advantages with respect to the electrochemical reaction kinetics[8−11] and the insignificance of the transient electrodic response.[9] The dispersed systems permit an extension of the concepts used in bipolar fluidized bed electrodes[12,13] to the area of microelectrodes. The possibility of carrying out electrochemical reactions at considerable rates in poorly conducting media by means of bipolar electrolysis with dispersions of conducting particles provides motivation for the development of the electrotechnology of dispersed systems. For example, the industrial application of the "superfast electrophoresis" effect,[14] which is based on the specific bipolar behavior of metallic particles[15] or ion-exchanger particles,[16] illustrates the relevance of understanding the bipolar properties of the conducting substrate|electrolyte solution interface. Recently, we have emphasized the fundamental importance of bipolar faradaic depolarization within the new context of streaming potentials generated by metals in electroinactive and electroactive electrolytes.[17] We demonstrated that, in certain circumstances, macroscopic bodies of planar geometry placed in a lateral electric field can behave as bipolar electrodes.[17,18] The propensity of the metallic surface to depolarization under the influence of a lateral electric field in the solution explains the feasibility of electrokinetic measurements for the investigation of double-layer properties of conducting materials. Measurements of the bipolar current have been performed[17,18] for irreversible and reversible systems for which the electron-transfer kinetics and diffusive mass transfer, respectively, govern the faradaic processes. A theoretical treatment based on the first-order approximation of a linear distribution of the potential or, equivalently, on the assumption of a homogeneous field along the bipolar electrode is also available.[17,18] This treatment, though useful for a qualitative understanding of the electrochemical and electrokinetic implications of the bipolar phenomenon, is oversimplified because of the intrinsic coupling between the potential distribution and the position-dependent faradaic current. In this paper, we rigorously tackle the pertinent field−current interrelation that is of importance for both irreversible and reversible electrode processes. We present analytical and numerical approaches to account for the nonlinear potential distribution and for the corresponding bipolar current. The theoretical results for planar symmetry successfully interpret experimental data for gold and aluminum surfaces in the presence and absence of a reversible redox couple. The analysis also provides a rigorous theoretical basis for the quantitative understanding of faradaic depolarization as an interfering element in the study of electrokinetic properties of conducting bodies. In these studies, the bipolar electrodic process arises from enhanced tangential flow

* To whom correspondence should be addressed.
† Wageningen University.
‡ NIZO Research Institute.
§ Universitat de Lleida.

10.1021/jp022459g CCC: $25.00
Published on Web 04/04/2003

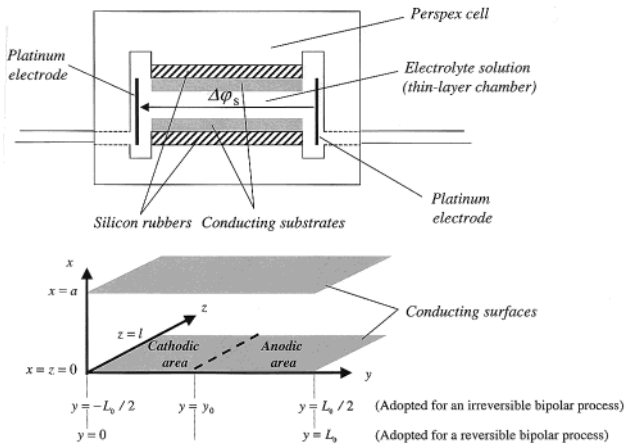

Figure 1. (Top) Schematic representation of the thin-layer cell. (Bottom) Geometric sketch of the coordinate system chosen for the formalism describing the bipolar behavior of the planar surfaces.

of the electrolyte solution along the conducting surface. The implications for the electrophoretic mobility of metallic particles and the collapse of the streaming potential of metallic surfaces in the presence of electroactive species will be discussed in detail elsewhere.

2. Definition of the Coordinate System, Notation

The coordinate system is defined in Figure 1. The distance between the two metallic electrodes in the flat capillary cell is a, the length of the metallic surface is L_0, and its width is l. A potential difference, denoted as $\Delta\varphi_s$, is applied across the long side of the thin-layer cell (y axis) between two auxiliary electrodes placed just outside the thin-layer chamber. In a scanning experiment, the value of $\Delta\varphi_s$ is systematically varied with time t according to the relation

$$\Delta\varphi_s(t) = \nu \times t \tag{1}$$

where ν is the scan rate (V s^{-1}). The bipolar faradaic current I_f at the metal|solution interface is carried by two redox couples denoted as Ox_a/R_a and Ox_c/R_c, where the subscripts a and c pertain to the anodic and cathodic processes, respectively (section 4). In the case where the current is carried by the same redox couple (section 5), the oxidized and reduced forms are denoted as Ox and R, respectively. The solution contains an electrolyte of given concentration c_s assumed to be in excess over the redox species. The solution conductivity in the thin-layer cell is denoted as K^L (Ω^{-1} m^{-1}) and is assumed to be constant with time t. So-called conductivity curves refer to plots of the overall current I, composed of the conduction current I_Ω and the bipolar faradaic current I_f, as a function of $\Delta\varphi_s$.

3. Expression of the Coupling between Electric Field and Faradaic Current

Considering the symmetry of the problem, the electric field and the faradaic current can be considered to be independent of the variable z, i.e., edge effects can be neglected. The explicit expression for the local potential $V(x,y,t)$, which denotes the potential of the solution at the positions x, y and given time t with respect to the (equipotential) metallic surface, is related to the magnitude of the local field, denoted as $E(x,y,t)$ (not to be confused with the common potential notation in electrochemistry)

$$E(x,y,t) = -\left(\frac{\partial V(x,y,t)}{\partial y} + \frac{\partial V(x,y,t)}{\partial x}\right) \tag{2}$$

In the following, we shall neglect the change of potential (and field) and the corresponding ionic charge distribution associated with the interfacial electric double layer (x direction). This assumption is justified provided that the condition $2\kappa^{-1} \ll a$ is fulfilled, where κ^{-1} is the Debye length characterizing the extension of the interfacial double layer. The correctness of this neglect for the systems modeled in this paper is in agreement with the choice made for the electrolyte concentration c_s. For illustration, in the range $c_s = (10^{-4})-1$ M, $2\kappa^{-1}/a \approx (3 \times 10^{-4})-(3 \times 10^{-6})$ ($a = 0.2$ mm). Therefore one can legitimately write the potential and the field as functions of y and t only (the derivative of V with respect to x in eq 2 is not taken into account). To find $E(y,t)$, let us consider an infinitesimally small volume element of the cell as pictured in Figure 2. This volume contains the electrolyte located between the positions y and $y + dy$. An ohmic current enters the considered volume element at y and leaves it at $y + dy$. A faradaic current with density j (A m^{-2}), which results from charge transfer between the solution and the conducting surfaces, enters the volume as a transversal current through the yz plane. In contrast to the common electrochemical situation, the flow of electrons associated with this faradaic current is perpendicular to the direction of the externally applied electric field. For an irreversible process under conditions of relatively weak faradaic depolarization, the chemical composition of the solution between the plates remains essentially constant (section 4). This is also true for the reversible case (section 5), provided that there is an excess of supporting electrolyte over the electroactive compounds. The field is considered to be established instantaneously. The electroneutrality condition for the elementary slice of volume $a \times l \times dy$ is

$$-aK^L \frac{\partial E(y,t)}{\partial y} + 2j(y,t) = 0 \tag{3}$$

Equation 3 defines the *intrinsic* relation between the faradaic current and the electric field at any position y along the surface and any time t. In the situation where $j = 0$ (no depolarization), eq 3, combined with eq 2, reduces to the common one-dimensional Poisson equation for an electroneutral medium

$$\frac{d^2V(y,t)}{dy^2} = 0 \tag{4}$$

Solution of eq 4 leads to a linear profile of the potential, i.e., a constant electric field. Once the dependence of j on the position is known, the electric field distribution, and hence the potential profile along the capillary cell, can be calculated with eq 3. We shall analyze the cases in which (i) the electron-transfer reaction at the bipolar metal|electrolyte interface is very slow compared to mass transport (the totally irreversible case) and (ii) the bipolar electrolytic processes are purely mass-transport-limited, i.e., electrochemically reversible.

4. Irreversible Bipolar Redox Process

4.1. Expressions of the Field Distribution and the Bipolar Current. The spatial variation of the solution potential $V(y,t)$ gives rise to an oxidation reaction at one side of the surface and a concomitant reduction reaction at the other side, as given by

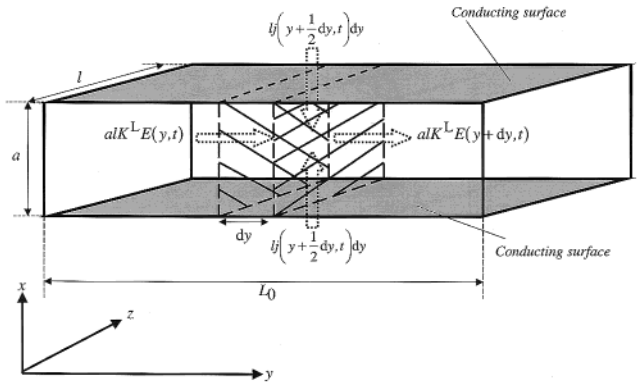

Figure 2. Schematic picture illustrating the coupling (eq 3 in the text) between the electric field E and the transversal faradaic current flow j at a given time t (or given potential $\Delta\varphi_s$) and position y.

$$R_a \rightarrow Ox_a + n_a e^- \tag{5a}$$

$$Ox_c + n_c e^- \rightarrow R_c \tag{5b}$$

with n_a and n_c denoting the numbers of electrons involved in eqs 5a and 5b, respectively. The anodic and cathodic current densities are denoted by j_a and j_c, respectively (A m^{-2}). In the irreversible case with the interfacial charge-transfer kinetics controlling the rates of the reactions, j_a and j_c are usually expressed by the so-called Butler−Volmer expressions[19]

$$j_a(y,t) = j_{0_a} \exp[-r_a f(V(y,t) - V_a^0)] \tag{6}$$

$$j_c(y,t) = -j_{0_c} \exp[r_c f(V(y,t) - V_c^0)] \tag{7}$$

with f, r_a, and r_c defined by

$$f = \frac{F}{RT} \tag{8}$$

$$r_a = n_a(1 - \alpha_a) \tag{9}$$

$$r_c = n_c \alpha_c \tag{10}$$

where α_a and α_c denote the transfer coefficients for the oxidation and the reduction reactions, respectively; j_{0_a} and j_{0_c} are the corresponding apparent exchange current densities; V_a^0 and V_c^0 are the standard potentials of Ox_a/R_a and Ox_c/R_c, respectively, with opposite sign (because here we consider the potential of the solution with respect to the metal surface); F is the Faraday constant; R is the gas constant; and T is the temperature. By analogy with electrochemical convention, the mixed potential V_m[20,21] is the potential at which the net local current ($j_a + j_c$) is zero

$$j_a(V_m) = -j_c(V_m) \tag{11}$$

It follows from eqs 6 and 7 that

$$V_m = \frac{\ln\left(\frac{j_{0_a}}{j_{0_c}}\right) + f(r_c V_c^0 + r_a V_a^0)}{f(r_c + r_a)} \tag{12}$$

The position at which V equals V_m is indicated as y_0. For the case of two totally irreversible reactions, we can neglect the local anodic and cathodic currents for $V > V_m$ and $V < V_m$, respectively. Using the properties of the exponential function, differentiation of eq 3 with respect to y and combination of the results with eqs 6 and 7 allows explicit expression of the field distribution for the anodic and cathodic areas by the following nonlinear differential equations of second order

$$y > y_0(t): \qquad \frac{\partial^2 E(y,t)}{\partial y^2} - r_a f \frac{\partial E(y,t)}{\partial y} E(y,t) = 0 \tag{13}$$

$$y < y_0(t): \qquad \frac{\partial^2 E(y,t)}{\partial y^2} + r_c f \frac{\partial E(y,t)}{\partial y} E(y,t) = 0 \tag{14}$$

which we write in concise form as

$$\frac{\partial^2 E(y,t)}{\partial y^2} + \epsilon_{a,c} r_{a,c} f \frac{\partial E(y,t)}{\partial y} E(y,t) = 0 \tag{15}$$

where $\epsilon_a = -1$ for $y > y_0(t)$ (anodic area) and $\epsilon_c = +1$ for $y < y_0(t)$ (cathodic area). Solving eq 15 requires two boundary conditions for the field, or equivalently for the potential (see eq 2). Because the surface of the metallic conductor is an equipotential plane, the total applied potential drop must comply with the condition

$$V(-L_0/2,t) - V(L_0/2,t) = \Delta\varphi_s(t) \tag{16}$$

As a consequence of eq 11, the position $y_0(t)$ is defined by

$$-\int_{-L_0/2}^{y_0(t)} j_c(y,t)\, dy = \int_{y_0(t)}^{L_0/2} j_a(y,t)\, dy \tag{17}$$

which stands for the condition of no charge accumulation in the overall bipolar conducting substrate. Each integral of eq 17 can be expressed as a function of the field by integration of the differential eq 3 so that the second searched boundary condition can be simply rewritten as

$$E(-L_0/2,t) = E(L_0/2,t) \tag{18}$$

Equation 15 can be easily integrated to give

$$\frac{\partial E(y,t)}{\partial y} + \frac{1}{2}\epsilon_{a,c} r_{a,c} f E(y,t)^2 = C(t) \tag{19}$$

where $C(t)$ is a constant (independent of position). $C(t)$ can be calculated at the particular position $y = y_0(t)$

$$C(t) = k_{a,c} + \frac{1}{2}\epsilon_{a,c} r_{a,c} f E(y_0(t),t)^2 \tag{20}$$

where the constant $k_{a,c}$ is defined by

$$k_{a,c} = -\frac{2\epsilon_{a,c} j_{0_{a,c}}}{aK^L} \exp[\epsilon_{a,c} r_{a,c} f(V_m - V_{a,c}^0)] \tag{21}$$

The differential eq 19 can be solved by integrating over the field from $E(y_0(t),t)$ to $E(y,t)$, i.e., over the space from $y_0(t)$ to y. After simple manipulation, it gives

$$\int_{E(y_0(t),t)}^{E(y,t)} \frac{dE(y,t)}{E(y,t)^2 - [E(y_0(t),t)^2 - \Lambda_{a,c}]} = -\frac{1}{2}\epsilon_{a,c} r_{a,c} f \int_{y_0(t)}^{y} dy \tag{22}$$

where $\Lambda_{a,c}$ (positive) is given by

$$\Lambda_{a,c} = \frac{2k}{r_{a,c} f} \tag{23}$$

and $k = |k_{a,c}|$. Let us consider the case where $E(y_0(t),t)^2 > \Lambda_{a,c}$, which typically holds for relatively high electrolyte concentrations (high K^L) and/or relatively low $j_{0_{a,c}}$. Then, the inequality $E(y,t)^2 > [E(y_0(t),t)^2 - \Lambda_{a,c}]$ is always verified, and the solution of eq 22 can be written as

$$E(y,t) = [E(y_0(t),t)^2 - \Lambda_{a,c}]^{1/2} \coth\left\{\mu_{a,c}(t) + \frac{1}{2}\epsilon_{a,c} r_{a,c} f[E(y_0(t),t)^2 - \Lambda_{a,c}]^{1/2}(y - y_0(t))\right\} \quad (24)$$

with the dimensionless quantity $\mu_{a,c}(t)$ defined by

$$\mu_{a,c}(t) = \coth^{-1}\left\{\frac{E(y_0(t),t)}{[E(y_0(t),t)^2 - \Lambda_{a,c}]^{1/2}}\right\} \quad (25)$$

The potential is then determined by spatial integration of the field from $y_0(t)$ to y (eq 2). The result is

$$V(y,t) - V_m = -\frac{2\epsilon_{a,c}}{r_{a,c} f} \ln\left\{\frac{\sinh\left\{\mu_{a,c}(t) + \frac{1}{2}\epsilon_{a,c} r_{a,c} f[E(y_0(t),t)^2 - \Lambda_{a,c}]^{1/2}(y - y_0(t))\right\}}{\sinh(\mu_{a,c}(t))}\right\} \quad (26)$$

The expression of $j_{a,c}(y,t)$ follows directly from relation 26 because eqs 6 and 7 can be rearranged in the form

$$j_{a,c}(y,t) = -\frac{ka\epsilon_{a,c}K^L}{2} \exp[\epsilon_{a,c} r_{a,c} f(V(y,t) - V_m)] \quad (27)$$

The bipolar current I_f equals the integral of the local anodic or cathodic current over the relevant surface area,[17,18] so that the analytical expression of the conductivity curve is given by

$$I_f(\Delta\varphi_s(t)) = lkaK^L\epsilon_{a,c} \times \int_{-\epsilon_{a,c}L_0/2}^{y_0(t)} \left\{\frac{\sinh(\mu_{a,c}(t))}{\sinh\left\{\mu_{a,c}(t) + \frac{1}{2}\epsilon_{a,c} r_{a,c} f[E(y_0(t),t)^2 - \Lambda_{a,c}]^{1/2}(y - y_0(t))\right\}}\right\}^2 dy \quad (28)$$

To explicitly calculate the potential, field and local current profiles as well as the overall faradaic current, the two parameters $E(y_0,t)$ and $y_0(t)$ remain to be determined as a function of the known input variables. The two additional equations required are provided by the boundary conditions on $\Delta\varphi_s(t)$ and on $y_0(t)$, i.e., eqs 16 and 17/18, respectively.

Equation 26 can be combined with eq 16 to yield

$$\Delta\varphi_s(t) = \frac{2}{r_c f} \ln\left\{\frac{\sinh(\mu_c(t))}{\sinh\left\{\mu_c(t) - \frac{1}{2}r_c f[E(y_0(t),t)^2 - \Lambda_c]^{1/2}\left(\frac{L_0}{2} + y_0(t)\right)\right\}}\right\} + \frac{2}{r_a f} \ln\left\{\frac{\sinh(\mu_a(t))}{\sinh\left\{\mu_a(t) - \frac{1}{2}r_a f[E(y_0(t),t)^2 - \Lambda_a]^{1/2}\left(\frac{L_0}{2} - y_0(t)\right)\right\}}\right\} \quad (29)$$

and using eq 18, eq 24 can be formulated as

$$\frac{\coth(\mu_c(t))}{\coth(\mu_a(t))} = \frac{\coth\left\{\mu_c(t) - \frac{1}{2}r_c f[E(y_0(t),t)^2 - \Lambda_c]^{1/2}\left(\frac{L_0}{2} + y_0(t)\right)\right\}}{\coth\left\{\mu_a(t) - \frac{1}{2}r_a f[E(y_0(t),t)^2 - \Lambda_a]^{1/2}\left(\frac{L_0}{2} - y_0(t)\right)\right\}} \quad (30)$$

Numeric resolution of the nonlinear system composed of eqs 29 and 30 provides, for different times t, and hence different $\Delta\varphi_s(t)$, the parameters $E(y_0(t),t)$ and $y_0(t)$.

For the cases where, even at high $\Delta\varphi_s$, $E(y_0(t),t)^2 < \Lambda_{a,c}$, the potential and field distributions are given by

$$E(y,t) = [\Lambda_{a,c} - E(y_0(t),t)^2]^{1/2} \tan\left\{\mu_{a,c}(t) - \frac{1}{2}\epsilon_{a,c} r_{a,c} f[\Lambda_{a,c} - E(y_0(t),t)^2]^{1/2}(y - y_0(t))\right\} \quad (31)$$

$$V(y,t) - V_m = -\frac{2\epsilon_{a,c}}{r_{a,c} f} \ln\left\{\frac{\sec(\mu_{a,c}(t))}{\sec\left\{\mu_{a,c}(t) - \frac{1}{2}\epsilon_{a,c} r_{a,c} f[\Lambda_{a,c} - E(y_0(t),t)^2]^{1/2}(y - y_0(t))\right\}}\right\} \quad (32)$$

with

$$\mu_{a,c}(t) = \tan^{-1}\left\{\frac{E(y_0(t),t)}{[\Lambda_{a,c} - E(y_0(t),t)^2]^{1/2}}\right\} \quad (33)$$

The secant function is defined as $\sec(x) = 1/\cos(x)$, where x is any number. The expression for the bipolar current I_f follows as

$$I_f(\Delta\varphi_s) = lkaK^L\epsilon_{a,c} \times \int_{-\epsilon_{a,c}L_0/2}^{y_0(t)} \left\{\frac{\sec\left\{\mu_{a,c}(t) - \frac{1}{2}\epsilon_{a,c} r_{a,c} f[\Lambda_{a,c} - E(y_0(t),t)^2]^{1/2}(y - y_0(t))\right\}}{\sec(\mu_{a,c}(t))}\right\}^2 dy \quad (34)$$

Equations 29 and 30, enabling the determination of $E(y_0(t),t)$ and $y_0(t)$, become

$$\Delta\varphi_s(t) = \frac{2}{r_c f} \ln\left\{\frac{\sec\left\{\mu_c(t) + \frac{1}{2}r_c f[\Lambda_c - E(y_0(t),t)^2]^{1/2}\left(\frac{L_0}{2} + y_0(t)\right)\right\}}{\sec(\mu_c(t))}\right\} + \frac{2}{r_a f} \ln\left\{\frac{\sec\left\{\mu_a(t) + \frac{1}{2}r_a f[\Lambda_a - E(y_0(t),t)^2]^{1/2}\left(\frac{L_0}{2} - y_0(t)\right)\right\}}{\sec(\mu_a(t))}\right\} \quad (35)$$

$$\frac{\tan(\mu_c(t))}{\tan(\mu_a(t))} = \frac{\tan\left\{\mu_c(t) + \frac{1}{2}r_c f[\Lambda_c - E(y_0(t),t)^2]^{1/2}\left(\frac{L_0}{2} + y_0(t)\right)\right\}}{\tan\left\{\mu_a(t) + \frac{1}{2}r_a f[\Lambda_a - E(y_0(t),t)^2]^{1/2}\left(\frac{L_0}{2} - y_0(t)\right)\right\}} \quad (36)$$

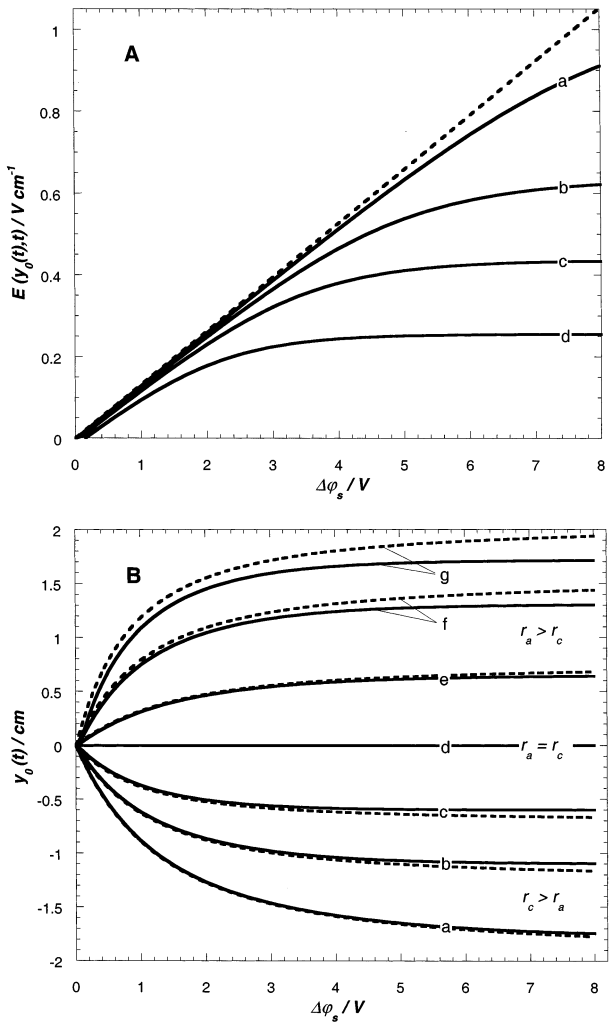

Figure 3. (A) Electric field $E(y_0(t),t)$ and (B) position $y_0(t)$ as a function of the total potential $\Delta\varphi_s$ applied across the thin-layer cell for different sets of kinetic parameters. The dashed lines result from the calculations of these quantities assuming a linear potential distribution (eq 4). Model parameters: $K^L = 10^{-1}\ \Omega^{-1}\ cm^{-1}$, $a = 0.17$ mm, $V_a^0 = 1.82$ V, $V_c^0 = 0.55$ V, $j_{0_a} = 10^{-7}$ A cm^{-2}, $j_{0_c} = 3 \times 10^{-6}$ A cm^{-2}. Panel A: $r_c = 1.1 \times 10^{-1}$ and (a) $r_a = 3.5 \times 10^{-2}$, (b) $r_a = 5.5 \times 10^{-2}$, (c) $r_a = 7.5 \times 10^{-2}$, (d) $r_a = 1.1 \times 10^{-1}$. Panel B: curves a−d as in panel A; for the other curves, $r_c = 5 \times 10^{-2}$ and (e) $r_a = 7.5 \times 10^{-2}$, (f) $r_a = 1.2 \times 10^{-1}$, (g) $r_a = 1.7 \times 10^{-1}$.

For the intermediate situations where $\Lambda_c < E(y_0(t),t)^2 < \Lambda_a$ (or $\Lambda_a < E(y_0(t),t)^2 < \Lambda_c$) relevant for bipolar electrodic processes with a strong asymmetry between anodic and cathodic charge transfer, the calculation of the electric parameters is possible by a cross use of the analytical expressions derived in this section for the field and potential position dependences.

4.2. Results and Discussion. Depending on the sign of the quantity $E(y_0(t),t)^2 - \Lambda_{a,c}$, $E(y_0(t),t)$ and $y_0(t)$ were consistently computed using eqs 29 and 30, 35 and 36 (or intermediate) for a few sets of kinetic parameters r_a, r_c, j_{0_a}, and j_{0_c} at constant electrolyte conductivity K^L. Some results are given in Figure 3. The order of magnitude chosen for the kinetic parameters is in agreement with values typical for the bipolar process occurring at aluminum, i.e., reduction of water at the cathodic side and anodic dissolution of the metallic phase at the other.[18] The calculations are shown for $\Delta\varphi_s$ up to 8 V. The choice of such high potentials is motivated by the typical range of electric fields encountered in the context of superfast electrophoresis at conducting particles: for particles of diameter 400 μm, the superfast effect is generated for a total potential difference of about 10 V along a single microsphere electrode.[15] To ensure the balance between the total anodic and cathodic currents, the position $y_0(t)$ at which there is no net current shifts to the anodic (cathodic) side for $r_c < r_a$ ($r_a < r_c$). One easily infers from eqs 30 and 36 that, for a kinetically symmetric system ($r_c = r_a$), y_0 remains independent of the applied potential and equal to 0. Figure 4A and B shows the spatial distributions of the potential and the faradaic current, respectively, along the bipolar electrode surface for a given set of kinetic parameters and for different $\Delta\varphi_s$. The corresponding conductivity curve [$I_f(\Delta\varphi_s)$ plot] calculated by means of the equations derived in the previous section is shown in Figure 4C. The results are also compared with those obtained assuming a linear potential distribution, as detailed in ref 18. The field and potential profile deviate from those obtained using the linear approximation when the bipolar current becomes significant compared to the ohmic current. This is realized by enlarging the kinetic parameters at constant conductivity K^L and/or gradually increasing $\Delta\varphi_s$ (Figures 3 and 4). The linear approximation leads to overestimation of the potentials $V(y,t)$ and, hence, to overestimation of the overall bipolar current I_f. As expected, both analyses correctly show the minimum overpotential (here about 1.5 V) thermodynamically required for the simultaneous occurrence of the anodic and cathodic reactions at the two sides of the surface. Owing to the exponential nature of the bipolar faradaic processes, the magnitudes of the local faradaic currents j_a and j_c grow strongly toward the extremities of the surface. The field (potential)−current correlation, as expressed by eq 3, is therefore the most pronounced at these positions, which results in the typical nonlinear patterns for the field and potential. The inaccuracy of the linear approximation for describing the distribution of the electric parameters at positions situated around y_0 is explained by the deviations of the computed values of $E(y_0(t),t)$ from those estimated on the basis of a linear potential profile.

Using the analytical expressions developed in the previous section, the bipolar current was also calculated for the gold|KNO_3 solution interface at different electrolyte concentrations, c_s for which the condition $2\kappa^{-1} \ll a$ is always fulfilled. For the range of applied values of $\Delta\varphi_s$, the bipolar process at gold is carried by the reduction and oxidation of water.[17] The conductivity curves are reported in Figure 5. The results are essentially the same as those obtained for aluminum bipolar electrodes. The higher the conductivity (or c_s), the lower the faradaic contribution to the total current, and the better the merging between the analysis as presented in section 4.1. and the linear approximation based on eq 4. Equations 28 and 34 tend to underestimate the overall measured current at low K^L, whereas the experimental results can still be fitted by the linear analysis. This can be understood by considering that, for moderate potentials, the local currents due to oxidation of the gold surface[22] are not taken into account, even though they probably play a role in the overall bipolar process, especially when the bulk conductivity is low. This is manifested in the difficulty in accurately determining the kinetic parameters at low electrolyte concentration from the measured voltammograms (deviations from the theoretical Tafel plots). Despite this complication, the two types of analysis give an acceptable picture of the conductivity curves. Similar conclusions hold for the irreversible bipolar process observed at aluminum surfaces. The inadequacy of the linear approach is the more apparent at higher $\Delta\varphi_s$. In the particular case where the electrode processes exhibit quasi-reversible behavior, we recognize that

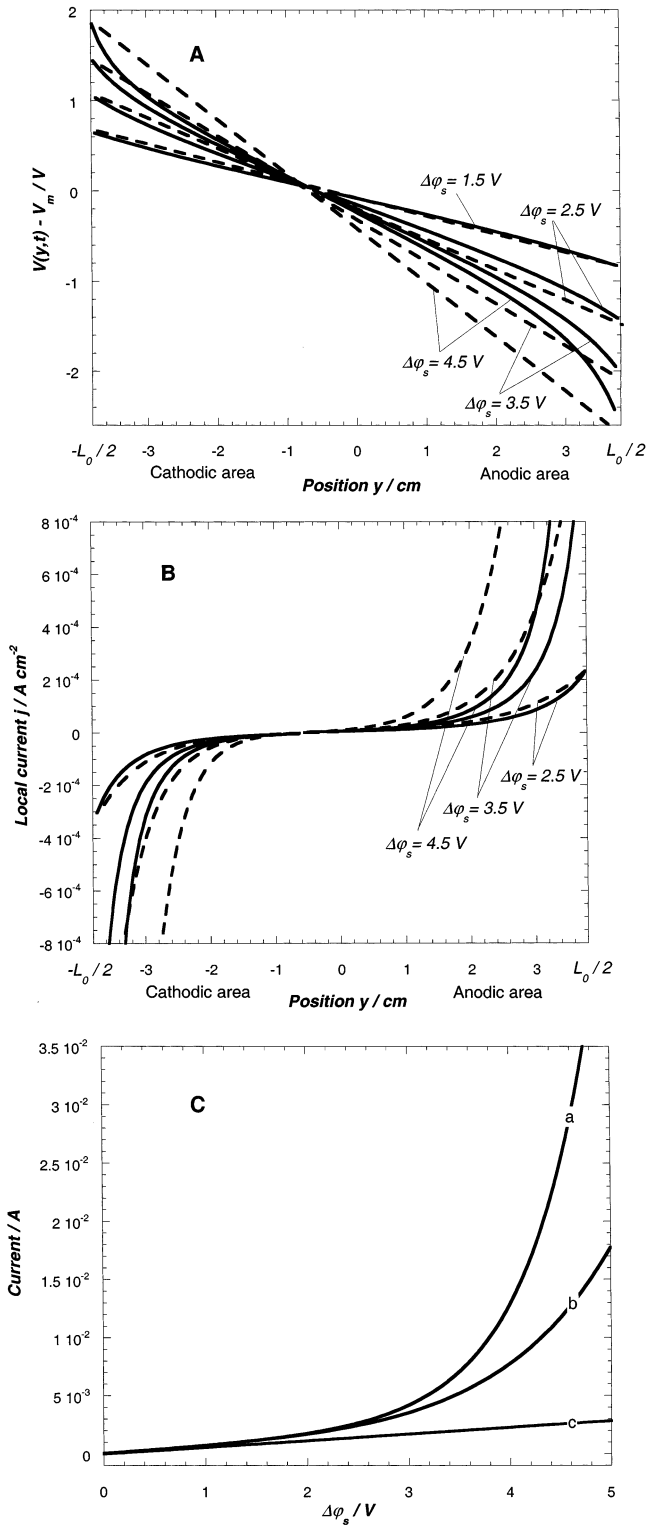

Figure 4. Spatial distributions of the (A) potential and (B) faradaic current at different $\Delta\varphi_s$, as specified in the figures. (C) Representation of the total current (ohmic + faradaic contributions) (a) assuming eq 4 and (b) calculated on the basis of eq 3. Curve c shows only the ohmic contribution to the total current. Model parameters: as in Figure 3 with $r_c = 1.1 \times 10^{-1}$ and $r_a = 7.5 \times 10^{-2}$.

the net current involves appreciable limitation from the finite rates of the forward and reverse charge-transfer processes, meaning that eqs 6 and 7 should be extended with the (smaller) cathodic and anodic terms, respectively. The results related to the potential and field profiles remain qualitatively the same as for the irreversible case.

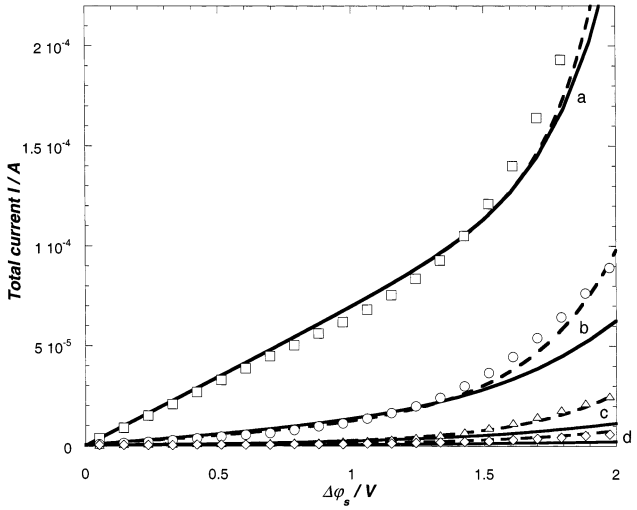

Figure 5. Experimental **(**points**)** and theoretical **(**solid lines) polarization plots for bipolar gold electrodes at different KNO_3 electrolyte concentrations, c_s. (a) $c_s = 10^{-1}$ M ($K^L = 11$ mΩ^{-1} cm^{-1}), (b) $c_s = 10^{-2}$ M ($K^L = 1.5$ mΩ^{-1} cm^{-1}), (c) $c_s = 10^{-3}$ M ($K^L = 160$ $\mu\Omega^{-1}$ cm^{-1}), (d) $c_s = 10^{-4}$ M ($K^L = 20$ $\mu\Omega^{-1}$ cm^{-1}). $a \approx 0.20$ mm. The potential was linearly scanned (0.03 V s^{-1}). The dashed lines refer to the theoretical treatment based on eq 4.

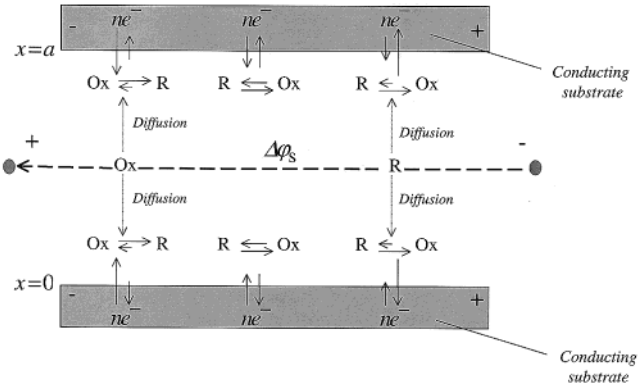

Figure 6. Schematic representation of the reversible bipolar process occurring in the thin-layer cell upon application of a potential drop $\Delta\varphi_s$ across the capillary. Diffusion of the redox components Ox (oxidized species) and R (reduced species) to/from the surfaces governs the faradaic processes.

5. Reversible Bipolar Redox Process

5.1. Expressions for the Local Faradaic Current and the Concentration Profile. If the bipolar current is carried via an electrochemically reversible reaction (fast electron transfer), the local currents along the bipolar surface (*y* dimension) are controlled by diffusion to/from the surface (*x* dimension) of the two electroactive species, now denoted as Ox for the oxidized form and R for the reduced form. The electrolyte solution is still assumed to contain an indifferent electrolyte in sufficient excess over the electroactive species. This ensures that diffusive mass transport prevails (migration of the redox species and its contribution to the ohmic current can therefore be neglected). In contrast to section 4, only one redox couple now generates the bipolar depolarization process. Figure 6 schematically depicts the situation typically encountered in the reversible case. Using the same definition for the electric potential as in the previous section (i.e., potentials in solution with respect to the metallic phase), the potential $V(y,t)$ is given by the Nernst relation

$$V(y,t) = V^0 - \frac{1}{nf}\ln\left[\frac{c_{Ox}(x=0,y,t)}{c_R(x=0,y,t)}\right] = V^0 - \frac{1}{nf}\ln\left[\frac{c_{Ox}(x=a,y,t)}{c_R(x=a,y,t)}\right] \quad (37)$$

where $c_{Ox}(x,y,t)$ and $c_R(x,y,t)$ stand for the concentrations of the oxidant Ox and reductant R at a given time t and position (x,y) and n is the number of electrons in the reaction $Ox + ne^- \leftrightarrow R$. V^0 is the negative of the standard potential of the redox couple Ox/R. The potential V^*, identified as the potential drop at the interface at $t = 0$ (before application of $\Delta\varphi_s$) does not depend on y and is related to the bulk concentrations c^*_{Ox}, c^*_R, and V^0 by

$$V^* = V^0 - \frac{1}{nf}\ln\left(\frac{c^*_{Ox}}{c^*_R}\right) \quad (38)$$

Calculation of the local current density $j(y,t)$ along the y axis at time t requires determination of the concentration profiles of the redox species within the capillary cell. Let us examine, e.g., the cathodic reaction and the profile of $c_{Ox}(x,y,t)$. Considering that, typically, $L_0 \gg a$ and $l \gg a$, the concentration polarization of Ox in the y and z directions can be neglected. Consequently, the faradaic current is limited by the diffusion of the species in the x direction, and $c_{Ox}(x,y,t)$ can be obtained by solving the diffusion equation

$$\frac{\partial c_{Ox}(x,y,t)}{\partial t} = D_{Ox}\frac{\partial^2 c_{Ox}(x,y,t)}{\partial x^2} \quad (39)$$

where D_{Ox} ($m^2\ s^{-1}$) is the diffusion coefficient of Ox. Resolution of eq 39 requires two spatial boundary conditions related to x (the system is spatially confined by the magnitude of the gap a) and one boundary condition related to the time. The latter is simply the initial condition

$$c_{Ox}(x,y,0) = c^*_{Ox} \quad (40)$$

which merely expresses the homogeneity of the solution at the start of the experiment. To define the spatial boundary conditions, we exploit the characteristic feature of reversible electrode reactions, that is, Nernstian equilibrium between the surface concentrations of the redox species and the potential $V(y,t)$. Assuming equal diffusion coefficients of Ox and R, i.e., $D_{Ox} = D_R = D$, the conservation of matter at the electrode surface $x = 0$ can be written as

$$c_{Ox}(x=0,y,t) + c_R(x=0,y,t) = c^*_{Ox} + c^*_R \quad (41)$$

and a similar expression holds at $x = a$. We note in passing that eq 41 is actually valid for every x because the total concentration of Ox and R at the boundaries is assumed to remain constant (protonation reactions of the redox species at the surfaces and/or in the bulk or other mechanisms likely to modify $c^*_{Ox} + c^*_R$ are not considered here). Combination of eqs 37 and 41 yields the two spatial boundary conditions

$$c_{Ox}(0,y,t) = c_{Ox}(a,y,t) = (c^*_{Ox} + c^*_R)f_{Ox}(y,t) \quad (42)$$

where the function f_{Ox} is defined by

$$f_{Ox}(y,t) = \frac{\exp[-nf(V(y,t) - V^0)]}{1 + \exp[-nf(V(y,t) - V^0)]} \quad (43)$$

The symmetry of the problem requires an extremum in the concentration profile of Ox at $x = a/2$. The ensuing condition

$$\partial c_{Ox}(x,y,t)/\partial x|_{x=a/2} = 0 \quad (44)$$

can be used in combination with eq 42 (at $x = 0$ or at $x = a$) and eq 40 in solving eq 39. The mathematical treatment of the set of eqs 39, 40, 42 and 43 substantially differs from that commonly applied within the semi-infinite planar diffusion approximation. In the present case, the notion of bulk concentration for the redox couple might vanish because of the small volume between the flat plates, and significant depletion might already occur (at $x = a/2$) for relatively short time t. The finite dimension of the capillary is taken into account in eq 42, which depends on one of the variables to be integrated (time t). To solve the problem, we use the Laplace transform with respect to the variable t. Using initial condition (40), eq 39 then becomes

$$s\bar{c}_{Ox}(x,y,s) - c^*_{Ox} = D\frac{\partial^2 \bar{c}_{Ox}(x,y,s)}{\partial x^2} \quad (45)$$

where the super bar denotes the transformed variable. A solution of eq 45 is

$$\bar{c}_{Ox}(x,y,s) = \frac{c^*_{Ox}}{s} + A(y,s)\exp(x\sqrt{s/D}) + B(y,s)\exp(-x\sqrt{s/D}) \quad (46)$$

where $A(y,s)$ and $B(y,s)$ are functions that are independent of x. Combination of eq 46, applied to the positions $x = 0$ and $x = a$, and the Laplace transform of eq 43 provides $A(y,s)$ and $B(y,s)$

$$A(y,s) = B(y,s)\exp(-a\sqrt{s/D}) = \frac{(c^*_{Ox} + c^*_R)\bar{f}_{Ox}(y,s) - c^*_{Ox}/s}{1 + \exp(a\sqrt{s/D})} \quad (47)$$

Equations 46 and 47 enable the explicit calculation of the local concentration gradients. For the two surfaces ($x = 0$ and $x = a$), we obtain

$$\frac{\partial \bar{c}_{Ox}(x,y,s)}{\partial x}|_{x=0} = -\frac{\partial \bar{c}_{Ox}(x,y,s)}{\partial x}|_{x=a} = \left[\frac{c^*_{Ox}}{s} - (c^*_{Ox} + c^*_R)\bar{f}_{Ox}(y,s)\right]\sqrt{\frac{s}{D}}\tanh\left(\frac{a}{2}\sqrt{\frac{s}{D}}\right) \quad (48)$$

Dividing by s yields a form for which the inverse Laplace transform is known. Use of the convolution integral[23] and tabulated functions[24] then leads to, e.g., for the surface at $x = 0$

$$\int_0^t \frac{\partial c_{Ox}(x,y,\tau)}{\partial x}|_{x=0}\,d\tau = \frac{4}{a}\int_0^t [c^*_{Ox} - (c^*_{Ox} + c^*_R)f_{Ox}(y,\tau)]\left\{\sum_{n=1}^{\infty}\exp\left[-(2n-1)^2\pi^2\frac{D}{a^2}(t-\tau)\right]\right\}d\tau \quad (49)$$

where τ is a dummy integration variable. Using the Leibniz theorem,[25] the concentration gradient at the surface $x = 0$ follows as

$$\frac{\partial c_{Ox}(x,y,t)}{\partial x}|_{x=0} = \frac{4}{a}\left\{[c^*_{Ox} - (c^*_{Ox} + c^*_R)f_{Ox}(y,0)]\left\{\sum_{n=1}^{\infty} \exp\left[-(2n-1)^2\pi^2\frac{D}{a^2}t\right]\right\} - (c^*_{Ox} + c^*_R)\int_0^t \frac{\partial f_{Ox}(y,t-\tau)}{\partial t}\left\{\sum_{n=1}^{\infty} \exp\left[-(2n-1)^2\pi^2\frac{D}{a^2}\tau\right]\right\} d\tau\right\} \quad (50)$$

Because we have assumed $D_{Ox} = D_R$, an expression comparable to eq 50 is obtained for the surface concentration gradient of species R.

The current density $j(y,t)$ for one bipolar electrode is related to the fluxes of Ox and R to/from the capillary surfaces by

$$j(y,t) = -nFD\left[\frac{\partial c_{Ox}(x,y,t)}{\partial x}\right]_{x=0} = nFD\left[\frac{\partial c_R(x,y,t)}{\partial x}\right]_{x=0} \quad (51)$$

where the sign convention of a negative reduction current is followed. Analytical expressions for the complete profiles of $c_{Ox}(x,y,t)$ and $c_R(x,y,t)$ can be obtained by following the route employed for solving analogous problems encountered within the context of heat conduction in solids.[26,27] A more straightforward procedure uses Laplace transformation of the concentration, eqs 46 and 47, in the form

$$\bar{c}_{Ox}(x,y,s) = \frac{c^*_{Ox}}{s} + \frac{1}{s}\left[s(c^*_{Ox} + c^*_R)\bar{f}_{Ox}(y,s) - \frac{c^*_{Ox} + c^*_R}{2} - \frac{c^*_{Ox} - c^*_R}{2}\right]\frac{\cosh[(x - a/2)\sqrt{s/D}]}{\cosh\left[\frac{a}{2}\sqrt{s/D}\right]} \quad (52)$$

By means of tabulated functions[25] and convolution integral,[24] the inverse transform of eq 52, and hence the concentration profile, is written as

$$c_{Ox}(x,y,t) = c^*_{Ox} + \int_0^t \left\{\left[(c^*_{Ox} + c^*_R)\frac{\partial f_{Ox}(y,t-\tau)}{\partial t} - \frac{c^*_{Ox} - c^*_R}{2}\delta(t-\tau)\right] \times \left\{1 + \frac{4}{\pi}\sum_{n=1}^{\infty}\frac{(-1)^n}{2n-1}\exp\left[-(2n-1)^2\pi^2\frac{D}{a^2}\tau\right]\cos\left[(2n-1)\pi\left(\frac{x}{a} - \frac{1}{2}\right)\right]\right\}\right\} d\tau \quad (53)$$

where $\delta(t)$ is the Dirac function. A similar expression can be obtained for $c_R(x,y,t)$.

5.2. Determination of the Field and Potential Distributions. Substitution of the current $j(y,t)$ as defined by eq 51 and eqs 43 and 50 into the differential eq 3 gives an (integro-)differential equation that must be solved to determine the profile of the field/potential across the capillary. In contrast to the irreversible case, which allowed analytical derivation, eq 3 now requires numerical treatment. In the following, we consider the integrodifferential equation written in terms of the potential $V(y,t)$. The methods employed for the discretization and resolution of the current problem are presented in the Appendix. The boundary equations are provided by eqs 16 and 18. With the coordinate system adopted within this section (Figure 1), the latter can also be written as

$$\frac{\partial V(y,t)}{\partial y}|_{y=0} = \frac{\partial V(y,t)}{\partial y}|_{y=L_0} \quad (54)$$

The equivalent of the mixed potential V_m for the irreversible case (see eq 12) is the Nernst potential V^* at which, by definition, $j = 0$ (eq 38). The potential−current coupling is subsumed in the function f_{Ox}, indicating that, at the surface, species Ox and R immediately adjust to the potential as dictated by the Nernst equation. For reversible reactions, neglect of double-layer effects is justified for cases where the thickness of the diffusion layer δ is large compared to the typical Debye length κ^{-1}, a condition that is always met in our experiments (sufficiently high salt concentrations).

5.3. Characteristic Features of the Conductivity Curves. Figure 7A and B shows typical curves for the spatial distributions of the faradaic current and potential, respectively, as calculated for different values of $\Delta\varphi_s$ and for a given set of redox concentrations satisfying $c^*_{Ox} = c^*_{Ox} = c^*$. For such a symmetric system, the position y_0 is independent of the applied field and is halfway along the surface ($y_0 = L_0/2$). For asymmetric systems ($c^*_{Ox} \neq c^*_R$), we have $y_0 < L_0/2$ for $c^*_R < c^*_{Ox}$ and $y_0 > L_0/2$ for $c^*_{Ox} < c^*_R$ (Figure 8). This is the counterpart of the asymmetry illustrated for the irreversible bipolar process when $r_c \neq r_a$ (see Figure 3B). In contrast to the situation examined in section 4, deviation of the potential distribution from a linear profile is apparent even for very weak applied lateral fields. This is a consequence of the absence of an activation barrier for electron transfer at the interface. As soon as a field is applied, the local potential $V(y,t)$ deviates from the Nernst potential V^* so that a faradaic current starts to flow. To qualitatively explain the dependence of the local current density j on $\Delta\varphi_s$, let us consider a particular position $y_p > L_0/2$ along the electrode (see Figure 7). As the field is gradually increased, the current $j(y_p,t)$ first increases because of the increase of the local potential drop $V(y_p,t)$ across the interface and the ensuing increase of the flux to the surfaces of the electrodes (Figure 9). This is related to the decrease in the surface concentration of the reduced species (as fixed by eq 37) with respect to the "bulk" value. Simultaneously, depletion of the electroactive species starts (Figure 9), and a diffusion layer (thickness δ) develops for the ongoing reactions at the two surfaces. Bulk depletion typically becomes significant for $\delta(y_p,t) \geq a/2$. From a given time t, the concomitant development of the diffuse layers at the two surfaces and the continuous decrease of the surface concentration results in a decrease of the concentration gradient at $y = y_p$, or stated otherwise, the current $j(y_p,t)$ passes through a maximum and then decreases to reach 0 in the limit $t \rightarrow \infty$ [$c_R(x=a/2,y_p,\infty) = 0$].

The *transient nature* of the diffusion process that develops during a linear sweep voltammetry experiment performed at a monopolar electrode leads to a characteristic peak-shaped current−potential curve.[28] The projection of this peak along the bipolar electrode surface, as dictated by the *nonlinear spatial distribution* of the potential/field in the solution, results in the characteristic patterns shown in Figures 7A and 8. For relatively long times t, the potential distribution increasingly tends to linearity owing to the decrease of the faradaic current, as caused by substantial depletion of the electroactive species. The increase of $\Delta\varphi_s$ (or time) at a given scan rate is accompanied by an accelerated compression of the projected voltammograms toward the position y_0 and by a decrease of the local peak currents resulting from depletion. The overall conductivity curves represent the *integration* of the anodic or cathodic current-space waves at varied $\Delta\varphi_s$. As a result of this operation, the curves

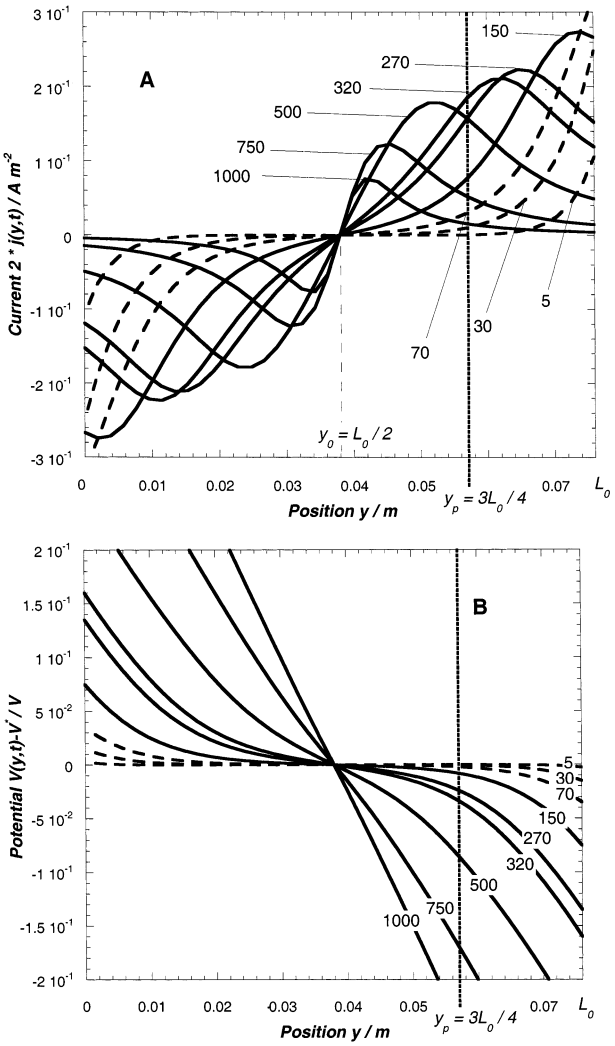

Figure 7. Spatial distribution of the (A) current and (B) potential at varied $\Delta\varphi_s$, as indicated (in mV) in the figures. Model parameters: $K^L = 3 \times 10^{-2}\ \Omega^{-1}\ cm^{-1}$, $a = 0.20$ mm, $V^0 = -233$ mV, $\nu = 50$ mV s^{-1}, $D = 10^{-9}\ m^2\ s^{-1}$, $n = 1$, $c^* = 10^{-4}$ M. The dashed curves correspond to the potentials where (substantial) depletion of the electroactive species does not occur at any position along the electrode.

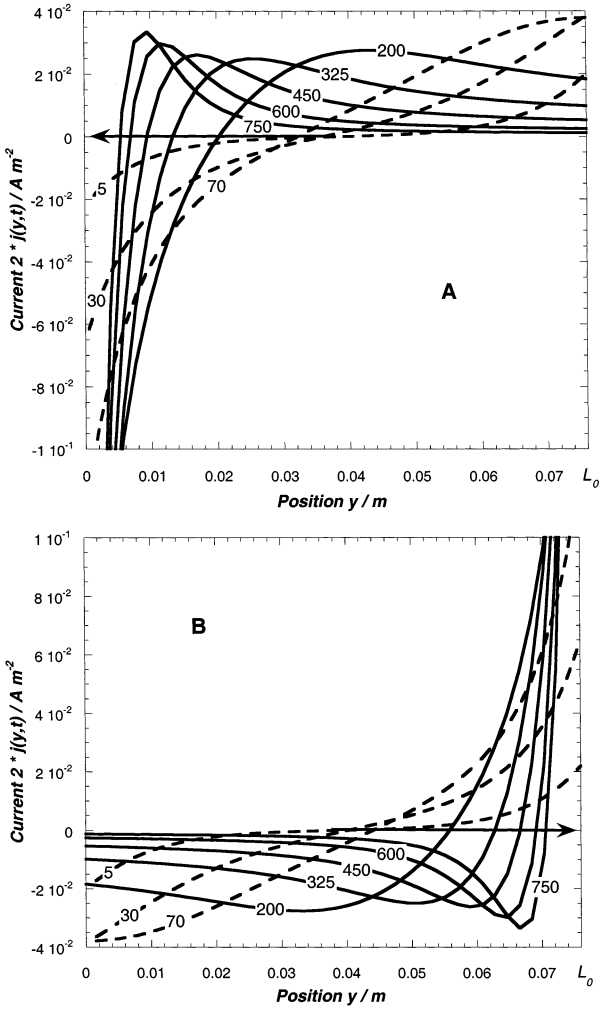

Figure 8. Projection along the bipolar electrode surface of the monopolar reversible waves for asymmetric redox systems at varied $\Delta\varphi_s$, as indicated (in mV) in the figure. Model parameters: as in Figure 7 except for the concentrations (A) $c^*_{Ox} = 10^{-3}$ M and $c^*_R = 10^{-5}$ M, (B) $c^*_{Ox} = 10^{-5}$ M and $c^*_R = 10^{-3}$ M. The dashed curves refer to the potentials for which substantial depletion of (A) the reduced species R and (B) the oxidized species Ox does not occur at any position along the electrode [$c_{Ox}(a/2,y,t) \approx c^*_{Ox}$]. The two systems lead to identical polarization plots. The arrows indicate the direction of shift of the position y_0 with time.

exhibit a maximum provided that sufficiently strong lateral fields are applied so as to induce noticeable transversal depletion of the redox species (Figure 10A). The higher the redox concentrations, the more delayed this phenomenon. This differs from monopolar voltammetry characteristics, which show depletion effects scaling with the bulk concentrations of Ox and R.[28] The fundamental difference between mono- and bipolar voltammetry becomes clear if the expression of the local current $j(y,t)$ as predicted from monopolar voltammetry theory is written explicitly with reversible species.[28] For a symmetric system

$$j(y,t) = nFc^*(\pi D\nu)^{1/2}\chi(V(y,t) - V^*) \qquad (55)$$

where χ is a function of position. For monopolar electrode polarization (the driving potential is perpendicular to the electrode surface), determination of χ was carried out both numerically and analytically.[29−33] Using eq 55 and the relation defining I_f, one obtains

$$I_f = 2nFlc^*(\pi D\nu)^{1/2}\int_{L_0/2}^{L_0} \chi(V(y,t) - V^*)\, dy \qquad (56)$$

Equation 56 indicates a linear relationship between I_f and c^*. The absence of linearity in our case (Figure 10B) is explained by the dependence of the potential distribution on the bulk concentration as formulated by eqs 3, 50, and 51. The higher the value of c^*, the more significant the bipolar faradaic current I_f with respect to the ohmic current, and the stronger the nonlinear coupling between the potential profile, as subsumed in the function χ, and the local current or, equivalently, the redox concentrations. Consequently, the error in the results expected on the basis of eq 56 together with a linear potential profile increases as $\Delta\varphi_s$ is increased at constant concentration and/or as the concentrations are increased at fixed $\Delta\varphi_s$, as illustrated in Figure 10B (K^L is kept constant). Similar reasoning holds for the dependence on the parameters D and ν (Figures 11 and 12, respectively). For sufficiently high ν, semi-infinite diffusion applies because the length of the diffusion layer decreases with increasing ν, as the ratio $2\delta/a$ becomes very small in that case. No depletion at $x = a/2$ occurs before the concentration at the conducting surfaces has dropped to 0. Hence, one should complete eq 56 by making the dependence of χ explicit in y, c^*, D, ν, K^L, and a. At every y, this χ function must satisfy the

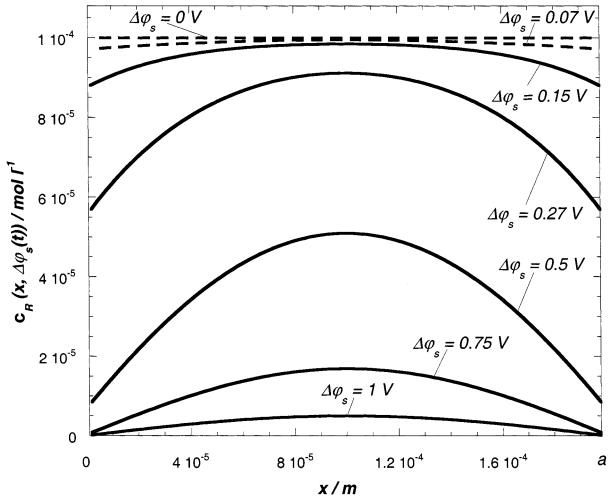

Figure 9. Concentration profile of the reduced species at the position $y = 3L_0/4$ and different applied potentials $\Delta\varphi_s$ (as mentioned in the figure). Model parameters as in Figure 7.

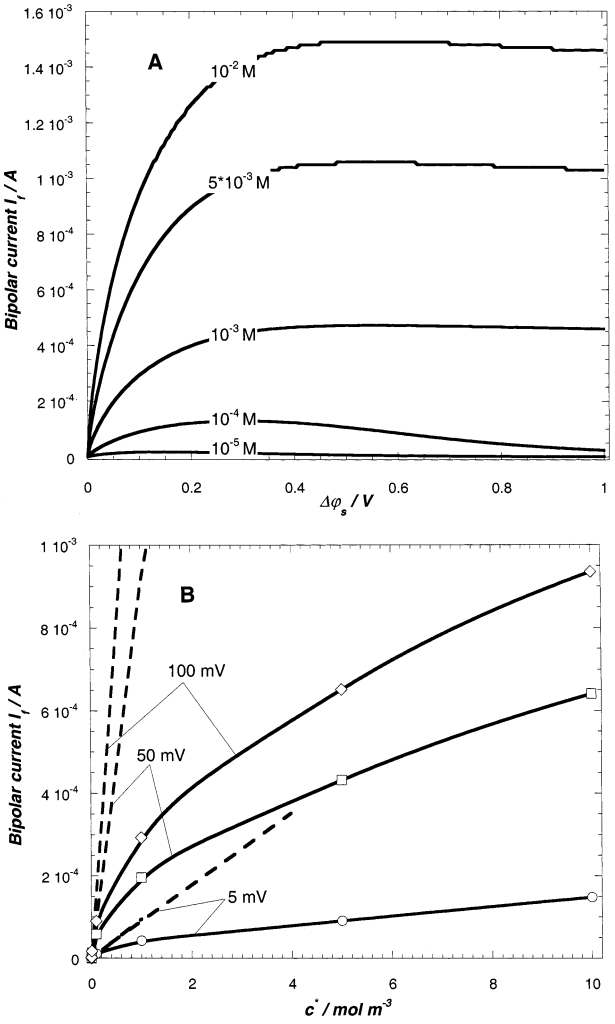

Figure 10. (A) Conductivity curves for different concentrations of the electroactive species c^* (symmetric redox system). c^* is specified in the figure. The other model parameters are the same as in Figure 7. (B) Deviation from the linear predictions (dashed lines) as yielded by eqs 4−56 at three different values of $\Delta\varphi_s$. The solid lines are only guides to the eye.

condition $\chi(V(y,t) - V^*) \leq \chi((y_0 - y)\Delta\varphi_s/L_0)$ because the linear field assumption systematically overestimates the local current and I_f. The extent of depletion depends on the thickness a between the electrodes. The higher a at given Ox and R concentrations, the higher the bipolar current I_f (because of higher local concentration gradients at the surface), and the higher the potential at which depletion appears, as illustrated in Figure 13 (a similar comment holds for Figure 12). For sufficiently high a and/or sufficiently low $\Delta\varphi_s$, the semi-infinite condition (which ascertains that regions sufficiently far from the electrode surfaces remain quasi-unperturbed by the ongoing experiment) is met, and I_f becomes independent of a.

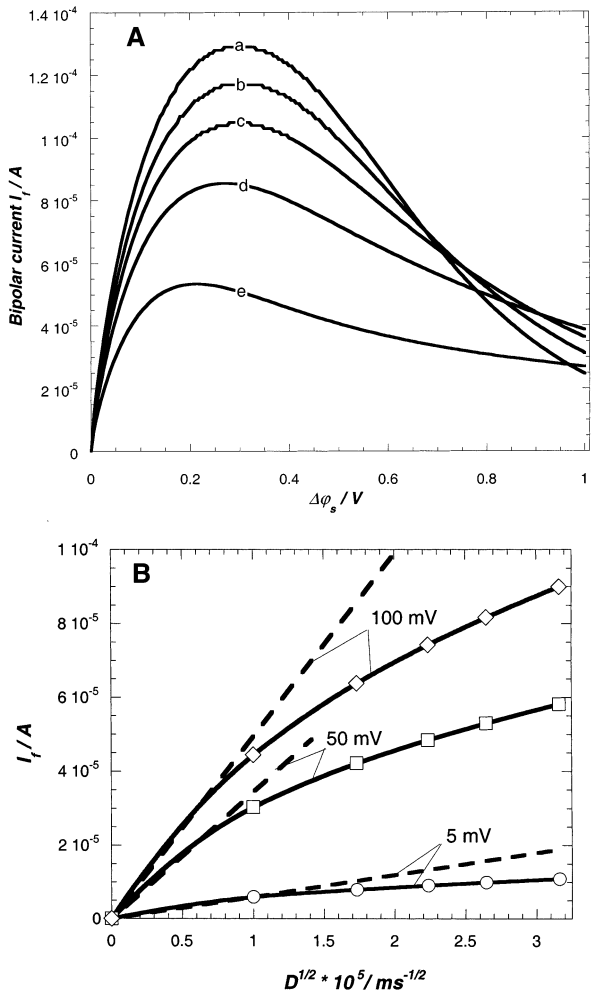

Figure 11. (A) Conductivity curves for different diffusion coefficients D (symmetric redox system). (a) $D = 10^{-9}$ m^2 s^{-1}, (b) $D = 7 \times 10^{-10}$ m^2 s^{-1}, (c) $D = 5 \times 10^{-10}$ m^2 s^{-1}, $D = 3 \times 10^{-10}$ m^2 s^{-1}, (e) $D = 1 \times 10^{-10}$ m^2 s^{-1}. The other model parameters are the same as in Figure 7. (B) Deviation from the linear predictions (dashed lines) as yielded by eqs 4−56 at three different values of $\Delta\varphi_s$. The solid curves are only guides to the eye.

In a previous study,[17] we demonstrated by (monopolar) cyclic voltammetry and electrochemical analysis performed on a gold rotating disk electrode (RDE) that the redox couple $Fe(CN)_6^{3-}$/$Fe(CN)_6^{4-}$ presents Nernstian behavior on gold, that is, the electron transfer is limited purely by diffusion to/from the surface. As such, this system enables validation of the theory presented in section 5. In Figure 14, we present a set of conductivity curves obtained for different redox concentrations and excess KNO_3 electrolyte. The results are in reasonable agreement with theoretical expectation. The difference between the experimental curves obtained for 10^{-3} Fe(III)/10^{-4} Fe(II) and 10^{-4} Fe(III)/10^{-3} Fe(II) is accounted for by a slight increase in the measured conductivity of the solution K^L (due to the difference in valency between the oxidized and reduced species).

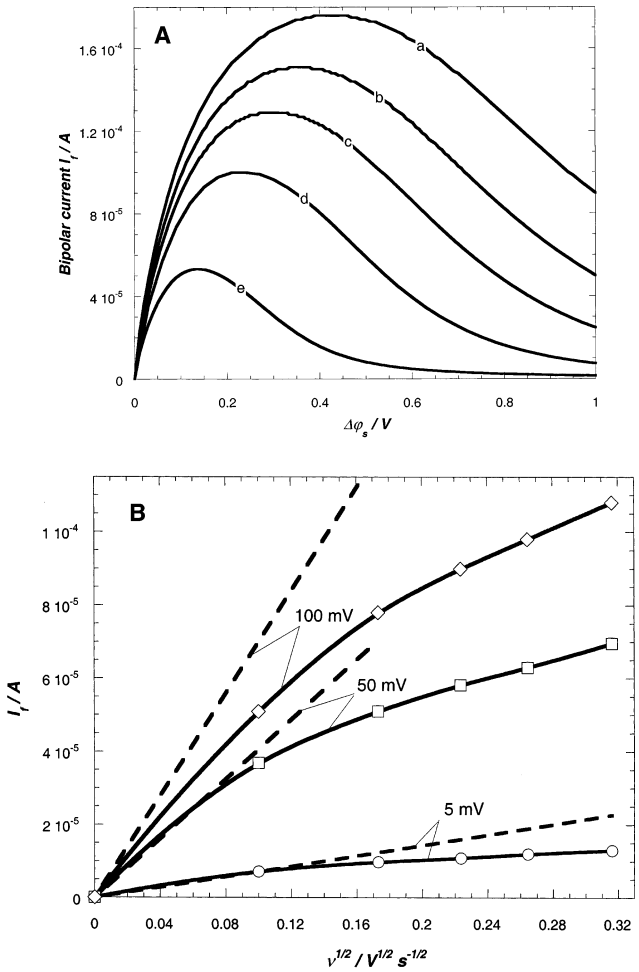

Figure 12. (A) Conductivity curves at different scan rates ν. (a) $\nu = 100$ mV s^{-1}, (b) $\nu = 70$ mV s^{-1}, (c) $\nu = 50$ mV s^{-1}, (d) $\nu = 30$ mV s^{-1}, (e) $\nu = 10$ mV s^{-1}. The other model parameters are the same as in Figure 7. (B) Deviation from the linear predictions (dashed lines) as yielded by eqs 4−56 at three different values of $\Delta\varphi_s$. The solid curves are only guides to the eye.

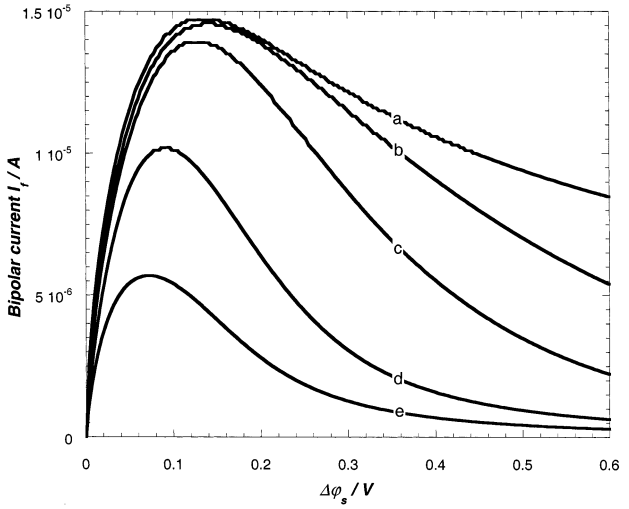

Figure 13. Conductivity curves at different a. (a) $a \geq 600$ μm (semi-infinite diffusion situation reached), (b) $a = 300$ μm, (c) $a = 200$ μm, (d) $a = 100$ μm, (e) $a = 50$ μm. The other model parameters are the same as in Figure 7.

This results in a decrease of the coupling field/current and therefore in an increase of I_f for the system of higher K^L. The trends expected from variation of the scan rate for given redox concentrations (see Figure 12) are also confirmed by experimental findings.

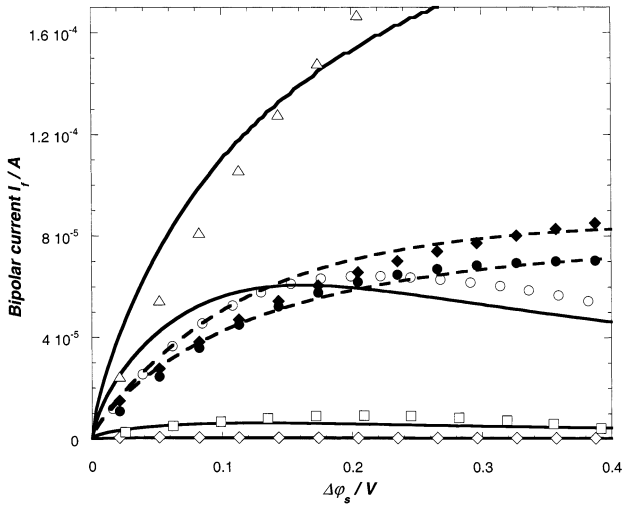

Figure 14. Comparison between experimental (points) and theoretical (curves) conductivity plots for different sets of electroactive concentrations. $V^0 = -233$ mV, $n = 1$, $D = 1.85 \times 10^{-10}$ m^2 s^{-1} [values derived from the rotating disk electrode (RDE) results[17]], $a \approx 0.20$ mm, $\nu = 30$ mV s^{-1}. Meanings of the symbols (1 M KNO_3): (◊) $c^* = 10^{-6}$ M ($K^L = 77$ mΩ^{-1} cm^{-1}), (□) $c^* = 10^{-5}$ M ($K^L = 78$ mΩ^{-1} cm^{-1}), (○) $c^* = 10^{-4}$ M ($K^L = 79$ mΩ^{-1} cm^{-1}); (0.1 M KNO_3) (△) $c^* = 10^{-3}$ M ($K^L = 12.9$ mΩ^{-1} cm^{-1}), (●) $c^*_{Ox} = 10^{-3}$ M and $c^*_R = 10^{-4}$ M ($K^L = 12.3$ mΩ^{-1} cm^{-1}), (♦) $c^*_{Ox} = 10^{-4}$ M and $c^*_R = 10^{-3}$ M ($K^L = 12.5$ mΩ^{-1} cm^{-1}). The theoretical dashed lines refer to the asymmetric redox systems.

6. Conclusions

We have presented a theoretical study for describing the faradaic depolarization effects that occur in a thin-layer cell of the type employed for electrokinetic analysis. A set of analytical equations governing the field distribution and the dependence of the bipolar current on the applied lateral potential difference is developed for the case where the current is carried by slow cathodic and anodic reactions (irreversible case). The case of a reversible bipolar process is also treated in detail. Mass transfer by diffusion of the electroactive species to/from the electrode surfaces is taken into account. Estimation of the ensuing bipolar current requires numerical computation of the intrinsic coupling between the profile of the field, as externally applied in the solution, and the spatial distribution of the faradaic current, in turn related to the local concentration profile of the redox species. The typical characteristics of the overall conductivity curves are described. Theoretical predictions are confirmed by experiments performed on gold electrodes with the electroactive couple $Fe(CN)_6^{3-}/Fe(CN)_6^{4-}$. In particular, transient effects due to development of diffusion layers, depletion of the electroactive species, and nonlinearity between the bipolar current and redox concentrations are well predicted.

The merging between experimental and theoretical results in the framework of the situation where the bipolar current is induced by an externally applied lateral field is promising for the interpretation of streaming potential data obtained on gold in the presence of electroactive compounds.[17] The quantitative interpretation of these electrokinetic results requires a rigorous analysis of the faradaic conduction phenomenon resulting from the interplay between the diffusion process, the field/current coupling, and the convection situation, as determined by hydrodynamic flow applied tangentially to the conducting surfaces. It allows for an appreciation of the dependence of the

electrokinetic potential on the total potential drop across the metal|solution interface, which can be electrochemically manipulated by the redox species in the solution. Although this type of investigation has become common in interfacial studies by atomic force microscopy, where the potential of the metallic phase is varied via an external electric circuit,[34−37] it has not yet been envisaged in the field of electrokinetics. The concepts elaborated in this paper are also useful for the quantitative interpretation of faradaic depolarization processes occurring in electrophoretic experiments performed on metallic particles. Rigorous analysis of the so-called superfast electrophoresis of such colloidal particles at low electrolyte concentration is needed. For these systems, the mass-transport-controlled space-charge formation (which is at the origin of the effect) resulting from the bipolar electrolysis requires theoretical analysis.

Acknowledgment. Dr. Josep Galceran and Dr. Jaume Puy from the Department of Chemistry at the University of Lleida (Spain) are acknowledged for their useful advice concerning section 5 of this paper.

Appendix

Descretization of the Reversible Charge-Transfer Problem (Eqs 3, 50, and 51 in the Text). The local faradaic current density (eqs 50 and 51) is written for two bipolar electrodes as

$$2j(y,t) = -\frac{8nFD}{a}\left\{[c^*_{Ox} - (c^*_{Ox} + c^*_R)f_{Ox}(y,0)]\sum_{n=1}^{\infty} \exp\left[-(2n-1)^2\pi^2\frac{D}{a^2}t\right] - (c^*_{Ox} + c^*_R)\int_0^t \frac{\partial f_{Ox}(y,t-\tau)}{\partial t}\left\{\sum_{n=1}^{\infty} \exp\left[-(2n-1)^2\pi^2\frac{D}{a^2}\tau\right]\right\} d\tau\right\} \quad (A1)$$

Discretization of the local current density with respect to time was performed by linear piecewise interpolation of the function f_{Ox}. Using the uniform convergence of the integral expression in eq A1, we obtain

$$2j(y,t_N) = -\frac{8nFD}{a}\left\{[c^*_{Ox} - (c^*_{Ox} + c^*_R)f_{Ox}(y,0)]\sum_{n=1}^{\infty} \exp\left[-(2n-1)^2\pi^2\frac{D}{a^2}t_N\right] - (c^*_{Ox} + c^*_R)\sum_{k=1}^{N}\frac{f_{Ox}(y,t_{N-k+1}) - f_{Ox}(y,t_{N-k})}{h}\sum_{n=1}^{\infty}\int_{t_{k-1}}^{t_k} \exp\left[-(2n-1)^2\pi^2\frac{D}{a^2}\tau\right] d\tau\right\} \quad (A2)$$

where $t_k = kh$, k is an integer satisfying $k \in [1, N]$, and h is the time step. After some rearrangement, one obtains

$$2j(y,t_N) = -\frac{8nFD}{a}\left\{(c^*_{Ox} + c^*_R)\frac{\alpha(N,h)}{h}f_{Ox}(y,0) + [c^*_{Ox} - (c^*_{Ox} + c^*_R)f_{Ox}(y,0)]\beta(N,h) + \frac{1}{h}(c^*_{Ox} + c^*_R)\sum_{j=1}^{N-1}[\alpha(N-j,h) - \alpha(N-j+1,h)]f_{Ox}(y,t_j) - \frac{1}{h}(c^*_{Ox} + c^*_R)\alpha(1,h)f_{Ox}(y,t_N)\right\} \quad (A3)$$

where α and β are the functions defined by

$$\alpha(k,h) = \sum_{n=1}^{\infty}\int_{t_{k-1}}^{t_k} \exp\left[-(2n-1)^2\pi^2\frac{D}{a^2}\tau\right] d\tau \quad (A4)$$

$$\beta(k,h) = \sum_{n=1}^{\infty} \exp\left[-(2n-1)^2\pi^2\frac{D}{a^2}t_N\right] \quad (A5)$$

Performing the integration in eq A4, α is rewritten as

$$\alpha(k,h) = \frac{a^2}{D\pi^2}[\gamma(k-1,h) - \gamma(k,h)] \quad (A6)$$

with γ given by

$$\gamma(k,h) = \sum_{n=1}^{\infty}\frac{1}{(2n-1)^2}\exp[-(2n-1)^2\theta(k,h)] \quad (A7)$$

and

$$\theta(k,h) = \pi^2\frac{D}{a^2}kh \quad (A8)$$

For the estimations of $\gamma(k,h)$ [and hence $\alpha(k,h)$] and $\beta(k,h)$, we use the following inequalities as conditions for convergence

$$|\gamma(k,h) - \sum_{n=1}^{L}\frac{1}{(2n-1)^2}\exp[-(2n-1)^2\theta(k,h)]| \le \frac{\exp[-(2L-1)^2\theta(k,h)]}{(2L-1)^2}\frac{\exp[-8L\theta(k,h)]}{1-\exp[-8L\theta(k,h)]} \quad (A9)$$

$$|\beta(k,h) - \sum_{n=1}^{P}\exp[-(2n-1)^2\theta(k,h)]| \le \exp[-(2P-1)^2\theta(k,h)]\frac{\exp[-8P\theta(k,h)]}{1-\exp[-8P\theta(k,h)]} \quad (A10)$$

where L and P are integers satisfying A9 and A10, respectively, and up to which the summations in eqs A7 and A5 are carried out. At this point of the analysis, the discretization in the space dimension remains to be done. For that purpose, we write $y_i = i\Delta y$ ($y_i \in [0,L_0]$), with $i \in [1, M]$ and Δy the space step. For convenience, we define the following quantities

$$\mathrm{term}(i,N) = -\frac{8nFD}{a^2K^L}\sigma(N,h,i)\Delta y^2 \quad (A11)$$

$$\sigma(N,h,i) = (c^*_{Ox} + c^*_R)\frac{\alpha(N,h)}{h}f_{Ox}(y_i,0) + [c^*_{Ox} - (c^*_{Ox} + c^*_R)f_{Ox}(y_i,0)]\beta(N,h) + \frac{1}{h}(c^*_{Ox} + c^*_R)\sum_{j=1}^{N-1}[\alpha(N-j,h) - \alpha(N-j+1,h)]f_{Ox}(y_i,t_j) \quad (A12)$$

$$\mathscr{R} = \frac{8nFD}{a^2hK^L}\alpha(1,h)\Delta y^2 \quad (A13)$$

Discretization of eq 3 (see text) in space leads to the following system of M nonlinear equations valid at every time t_N with the potentials at y_i as unknown variables

$$V(y_1,t_N) - V(y_M,t_N) - \Delta\varphi_s(t_N) = 0 \quad (A14)$$

$$i \in [2, M-1]: \quad V(y_{i+1},t_N) - 2V(y_i,t_N) + V(y_{i-1},t_N) + \mathscr{R}(c^*_{Ox} + c^*_R)f_{Ox}(y_i,t_N) + \text{term}(i,N) = 0 \quad \text{(A15)}$$

$$V(y_1,t_N) - V(y_2,t_N) - V(y_{M-1},t_N) + V(y_M,t_N) = 0 \quad \text{(A16)}$$

with the relation giving $f_{Ox}(y_i,t_N)$ as a function of the potential $V(y_i,t_N)$ (eq 43 in the text)

$$i \in [2, M]: \; f_{Ox}(y_i,t_N) - \frac{\exp[-nf(V(y_i,t_N) - V^0)]}{1 + \exp[-nf(V(y_i,t_N) - V^0)]} = 0 \quad \text{(A17)}$$

Equations A14 and A16 are derived from the boundary conditions associated with eq 3, that is, eqs 16−18 and 54. From the definition of the potential V^* (eq 38), one can write the particular relation $V(y_i,0) = V^*$, so that $f_{Ox}(y_i,0)$ is known. Subsequently, by iterating N from 1 to a chosen value N_{max} (depending on the potential range desired), resolution of the system A14−A17 enables determination of the potentials $V(y_i,t_N)_{i\in[1,M],N\in[1,N_{max}]}$ and consequently of the currents $j(y_i,t_N)_{i\in[1,M],N\in[1,N_{max}]}$ (eq A3). The ensuing bipolar current at a given N [or $\Delta\varphi_s(t_N)$] was then calculated by integrating the local faradaic currents by means of the trapeze method. The solutions of eqs A14−A17 were derived with a Newton−Raphson-type[38] numerical analysis.

References and Notes

(1) Hartland, M. A.; Spencer, A. J. M. *Trans. Inst. Chem. Eng.* **1963**, *41*, 328.
(2) Nadebaum, P. R.; Fahidy, T. Z. *Electrochim. Acta* **1975**, *20*, 715.
(3) King, C. J. H.; Lister, K.; Plimley, R. E. *Trans. Inst. Chem. Eng.* **1975**, *53*, 20.
(4) Goodridge, F.; King, C. J. H.; Wright, A. R. *Electrochim. Acta* **1977**, *22*, 347.
(5) Pletcher, D. *Industrial Electrochemistry*; Chapman and Hall Ltd.: London, 1982; p 162.
(6) Fleischmann, M.; Ghoroghchian, J.; Rolinson, D.; Pons, S. *J. Phys. Chem.* **1986**, *90*, 6392 and the citations of unpublished results by Rolinson, D. R.; Nowak, R. J.; Pons, S.; Fleischmann, M.; Ghoroghchian, J. and Ghoroghchian, J.; Pons, S.; Fleischmann, M.
(7) Fleischmann, M.; Ghoroghchian, J.; Pons, S. *J. Phys. Chem.* **1985**, *89*, 5530.
(8) Wightman, R. M. *Anal. Chem.* **1981**, *53*, 1125A.
(9) Howell, J. O.; Wightman, R. M. *Anal. Chem.* **1984**, *56*, 524.
(10) Bindra, P.; Brown, A. P.; Fleischmann, M.; Pletcher, D. *J. Electroanal. Chem.* **1975**, *58*, 31.
(11) Bindra, P.; Brown, A. P.; Fleischmann, M.; Pletcher, D. *J. Electroanal. Chem.* **1975**, *58*, 39.
(12) Fleischmann, M.; Goodridge, F.; King, C. J. H. Br. Patent Application 16 765, 1974.
(13) Goodridge, F.; King, C. J. H.; Wright, A. B. *Electrochim. Acta* **1977**, *22*, 1087.
(14) Dukhin, S. S. *Adv. Colloid Interface Sci.* **1991**, *35*, 173.
(15) Baran, A. A.; Mishchuk, N. A.; Prieve, D. C. *J. Colloid Interface Sci.* **1998**, *207*, 240.
(16) Baran, A. A.; Babich, Y. A.; Tarovsky, A. A.; Mischuk, N. A. *Colloids Surf.* **1992**, *68*, 141.
(17) Duval, J.; Huijs, G. K.; Threels, W. F.; Lyklema, J.; van Leeuwen, H. P. *J. Colloid Interface Sci.* **2003**, *260*(1), 95.
(18) Duval, J.; Kleijn, J. M.; van Leeuwen, H. P. *J. Electroanal. Chem.* **2001**, *505*, 1.
(19) Bard, A. J.; Faulkner, L. R. *Electrochemical Methods, Fundamentals and Applications*; John Wiley and Sons: New York, 1980; p 103.
(20) Wagner, C.; Traud, W. *Z. Elektrochem.* **1938**, *44*, 391.
(21) Spiro, M. In *The Physical Chemistry of Solutions*; Fenby, D. V., Watson, I. D., Eds.; Massey University: Auckland, New Zealand, 1983.
(22) Schmid, G. M. in *Standard Potentials in Aqueous Solution*; Bard, A. J., Parsons, R., Jordan, J., Eds.; Marcel Dekker: New York, 1985; p 313.
(23) Bard, A. J.; Faulkner, L. R. *Electrochemical Methods, Fundamentals and Applications*; John Wiley and Sons: New York, 1980; p 661.
(24) Churchill, R. V. *Operational Mathematics*, 2nd ed.; McGraw-Hill: New York, 1958.
(25) Kaplan, W. in *Advanced Calculus*, 2nd ed.; Addison-Wesley: Reading, Mass., 1973.
(26) Carslaw, H. S.; Jaeger, J. C. *Conduction of Heat in Solids*, 2nd ed.; Clarendon Press: Oxford, U.K., 1959.
(27) Duhamel in *Mémoire sur la méthode générale relative au mouvement de la chaleur dans les corps solides plongés dans les milieux dont la température varie avec le temps*, cf. *J. Ec. Polytech. (Paris), Cah. 22* **1833**, *14*, 20.
(28) Bard, A. J.; Faulkner, L. R. *Electrochemical Methods, Fundamentals and Applications*; John Wiley and Sons: New York, 1980; Chapter 6, p 213.
(29) Sevcik, A. *Collect. Czech. Chem. Commun.* **1948**, *13*, 349.
(30) Nicholson, R. S.; Shain, I. *Anal. Chem.* **1964**, *36*, 706.
(31) Reinmuth, W. H. *J. Am. Chem. Soc.* **1957**, *79*, 6358.
(32) Matsuda, H.; Ayabe, Y. *Z. Elektrochem.* **1955**, *59*, 494.
(33) Gokhshtein, Y. P. *Dokl. Akad. Nauk SSSR* **1959**, *126*, 598.
(34) Barten, D.; Kleijn, J. M.; Duval, J.; van Leeuwen, H. P.; Lyklema, J.; Cohen Stuart, M. A. *Langmuir* **2003**, *19* (4), 1133.
(35) Raiteri, R.; Grattarola, M.; Butt, H. J. *J. Phys. Chem.* **1996**, *100*, 16700.
(36) Döppenschmidt, A.; Butt, H. J. *Colloids Surf. A: Physicochem. Eng. Aspects* **1999**, *149*, 145.
(37) Hu, K.; Fan, F. R. F.; Bard, A. J.; Hillier, A. C. *J. Phys. Chem. B* **1997**, *101*, 8298.
(38) Press, W. H.; Teukolsky, S. A.; Vetterling, W. T.; Flannery, B. P. in *Numerical Recipes in Fortran, The Art of Scientific Computing*, 2nd ed.; Cambridge University Press: New York, 1986.